FEBS Letters

FEBS PRESS science publishing by scientists

RESEARCH ARTICLE

Neutrophil deficiency increases T cell numbers at the site of tissue injury in mice

Hajnalka Halász[1,2], Albert Bálint Papp[3,4], Lukács Sándor Lesinszki[5], Attila Mócsai[5], Tamás Varga[3], László Nagy[3] and Péter Gogolák[2]

1 Doctoral School of Molecular Cell and Immune Biology, Faculty of Medicine, University of Debrecen, Hungary
2 Department of Immunology, Faculty of Medicine, University of Debrecen, Debrecen, Hungary
3 Department of Biochemistry and Molecular Biology, Faculty of Medicine, University of Debrecen, Hungary
4 Doctoral School of Dentistry, Faculty of Dentistry, University of Debrecen, Hungary
5 Department of Physiology, Faculty of Medicine, Semmelweis University, Budapest, Hungary

Correspondence
P. Gogolák, Department of Immunology, Faculty of Medicine, University of Debrecen, 1. Egyetem Square, Debrecen, H-4032, Hungary.
Tel: +36 52 417 159
E-mail: gogy@med.unideb.hu

László Nagy and Péter Gogolák authors share last authorship.

(Received 23 March 2025, revised 28 May 2025, accepted 16 June 2025, available online 29 July 2025)

doi:10.1002/1873-3468.70126

Edited by Wilfried Ellmeier

During the investigation of muscle injury and regeneration in neutrophil-deficient mice, we observed unexpected changes in the cellular composition of tissue-infiltrating inflammatory cells. Neutrophil deficiency led to reduced macrophage infiltration and a striking increase in nonconventional $CD4^-$ $CD8^-$ (double-negative) αβ and γδ T cell numbers, peaking at Day 3 postinjury. In exploring the underlying mechanisms, we identified previously unrecognized cellular and tissue alterations, including bone marrow erythroid insufficiency and compensatory extramedullary hematopoiesis accompanied by splenomegaly. Using a thioglycolate-induced peritonitis model, we further demonstrated that elevated T-cell numbers reflect a general inflammatory response in neutrophil-deficient mice. Our findings suggest that this model provides a valuable platform for investigating the properties and functions of rare nonconventional T cells in tissue injury and diverse inflammatory conditions.

Keywords: double-negative T cells; double-negative αβ T cells; extramedullary hematopoiesis; increased gamma-delta T-cell number; increased T-cell count; inflammation; neutrophil deficiency; splenomegaly; tissue injury; γδ T cells

Impact statement

Our studies demonstrate that neutrophil-deficient mice may provide a valuable model for investigating the roles and characteristics of non-conventional T cells in tissue inflammation and repair.

Genetically modified mice are commonly used for research, frequently serving as animal models of human diseases. The versatility and precision of these models make them invaluable in biomedical research and the ongoing quest to improve human health. Conditional gene knockout models in mice are advanced

Abbreviations
CTX, cardiotoxin 1; DAMP, damage-associated molecular pattern; DN, double-negative; Mcl1, the gene of the "Induced myeloid leukemia cell differentiation" anti-apoptotic protein; Mcl1ΔMyelo, The myeloid cell type-specific inactivation of the Mcl1 gene ($Lyz2^{Cre/Cre}Mcl1^{flox/flox}$ genotype); p.i., postinjury; PALS, peri arteriolar lymphatic sheath (in the spleen); rcf, relative centrifugal force (g); rpm, revolution/min; SAP, serum amyloid P component (pentraxin 2, acute-phase protein); TA, tibialis anterior (in the context of injured muscle); WT, wild-type (genotype).

FEBS Letters 599 (2025) 2644–2662 © 2025 The Author(s). *FEBS Letters* published by John Wiley & Sons Ltd on behalf of Federation of European Biochemical Societies.

genetic tools that can be used to selectively inactivate specific genes in particular tissues or at designated times during development. This approach minimizes unintended effects on other tissues and enables the study of gene functions in specific biological contexts. It is particularly valuable for investigating human diseases and enables the targeted elimination of specific cell types characterized by particular gene expressions without adversely affecting embryonic development. Consequently, researchers can investigate gene functions in defined tissues at specific developmental stages, minimizing the risk of embryonic lethality commonly associated with traditional gene knockout methods. The most commonly used technique is the Cre-loxP recombination system [1].

The Cre-loxP recombination system can be used to induce the selective depletion of the anti-apoptotic Mcl1 gene. Neutrophils express several pro-apoptotic members of the Bcl-2 family (such as Bax, Bad, Bak, Bid and Bik), and only a few anti-apoptotic proteins, such as Mcl-1 and A1 [2]. Mcl1 is essential for the survival of neutrophil granulocytes [2]. The Lyz2 (also known as LysM) gene promoter-driven expression of the Cre recombinase excises the loxP sequence-flanked (floxed) gene regions of the Mcl1 gene in cells that exhibit active lysozyme 2 expression. This process severely affects developing neutrophil granulocyte precursors after they begin synthesizing and storing lysozyme [2]. It induces severe neutropenia in homozygous $Lyz2^{Cre/Cre}Mcl1^{flox/flox}$ mice without directly affecting other immune cells and with mostly normal survival and fertility under conventional conditions [2,3]. Such mice are referred to in the literature as Mcl-$1^{-/-}$ or Mcl1ΔMyelo genotype mice [2,3]. We use the latter term in this article to refer to them (see also in Materials and Methods).

Neutrophil granulocytes undoubtedly play a crucial role in eliminating extracellular microorganisms [4]; besides, in recent decades, several additional roles of this cell type have begun to accumulate [5]. Through cell–cell interactions or by secreting cytokines, chemokines, or other factors, neutrophils can modulate the activation of several cell types [6–9]. The manner of their death also influences the function of different leukocytes in the affected tissue [10], as the cell types participating in their removal (e.g., macrophages) can significantly impact the fate of the affected tissue, involving remodeling and repair. Neutrophils can even have immunomodulatory effects on T- and B-lymphocytes [11,12].

We aimed to investigate the role of neutrophil granulocytes in muscle injury, the associated inflammation, and regeneration process by the help of Mcl1ΔMyelo mice. Tissue injuries and regeneration are strongly influenced by the immune system through the inflammatory and the subsequent resolving process [13,14]. Muscle injury in mice can be rapidly resolved due to its remarkable regenerative capacity [15]. One of the most widely used muscle injury models involves injecting Cobra (Naja sp.) venom component cardiotoxin 1 (CTX) into the tibialis anterior (TA) muscle of mice [16]. Intramuscular injection of CTX induces acute muscle fiber necrosis, resulting in rapid recruitment of inflammatory cells and culminating in inflammation.

Neutrophils are the first cell type to arrive in inflamed tissue from the circulation. In cases of injury or infection, they can be attracted directly by chemotactic materials (including DAMPs, alarmins) released from necrotic tissues [17–19]. Tissue sentinel cells (e.g., tissue-resident macrophages, mast cells, innate lymphoid cells) can also be activated by these materials and subsequently produce neutrophil-attracting chemokines [20]. In inflamed tissue, neutrophils secrete chemokines and pro-inflammatory cytokines to recruit blood-derived monocytes [21]. Immigrating monocytes differentiate into $Ly6C^{++}$ inflammatory monocytoid macrophages in injured tissue. These inflammatory cells produce inflammatory cytokines (e.g., TNF) that activate muscle stem cells (satellite cells) [22] in the injured muscle to proliferate and become myoblasts [23,24].

Neutrophil granulocytes can have both regeneration-prone and regeneration-delaying effects in sterile tissue injuries [25,26]. They influence these processes directly or indirectly. They can start to clear away necrotic tissue debris. In large numbers, they can confer high arginase activity, which can modulate even the function of T cells [27]. Later, they die by apoptosis. The decreased amount of necrotic debris and the large number of apoptotic neutrophils induce a switch in the differentiation program of the immigrating $Ly6C^{++}$ inflammatory macrophages during the efferocytosis process. The appearing reprogrammed $F4/80^{+}$ $Ly6C^{low}$ macrophages have resolving functions [28,29]. They can support the reparative phase of myogenesis following the initial proliferative phase by producing anti-inflammatory cytokines [30], influencing other tissue precursor cells—such as fibro-adipogenic precursor (FAP) cells—or secreting other bioactive materials that induce the formation of myofibers from myoblasts or mediate tissue revascularization [31].

We used CTX-induced injury as a model to compare the cellular events of the inflammation process between wild-type (WT) and neutrophil granulocyte-deficient Mcl1ΔMyelo mice. Our results shed light on unexpected effects of neutrophil depletion in tissue

inflammation and injury. Specifically, we found that the absence of neutrophils increases the number of T cells in injured, inflamed tissues.

Materials and methods

Mice

The Mcl1$^{\Delta Myelo}$ mouse strain was kindly provided by Attila Mócsai (A.M.), Department of Physiology, Faculty of Medicine, Semmelweis University, Budapest, Hungary. Maintenance of the mouse colonies and animal husbandry were conducted at the Laboratory Animal Facility, Life Science Building, University of Debrecen, Hungary. All animal experiments were performed in accordance with Hungarian and European regulations approved by the Animal Care and Use Committee of the University of Debrecen (DEMÁB) with permission number 16/2019/DEMÁB.

We aimed to compare an equal number of animals from different age groups, ensuring equal representation of both sexes in each experimental group. Neutrophil granulocyte-deficient Lyz2$^{Cre/Cre}$ Mcl1$^{flox/flox}$ mice, also known as *Lyz2*$^{tm1(cre)Ifo/tm1(cre)Ifo}$*Mcl1*$^{tm1Ywh/tm1Ywh}$ and referred to as Mcl1ΔMyelo mice, aged 2–4 months and on a C57BL/6 genetic background, were used in the experiments. These mice were bred under specific pathogen-free conditions [2,3]. For comparison, both nonfloxed (Lyz2$^{Cre/Cre}$ Mcl1$^{+/+}$) and heterozygous variants (Lyz2$^{Cre/Cre}$ Mcl1$^{flox/+}$) could serve as WT controls [2,3]. Since these mice can be bred in both homozygous and heterozygous forms, their genotypes were determined using allele-specific PCR (see in Supporting Information section, Supplementary Materials and Methods, Fig. S1).

Genotyping

Total DNA was extracted from tissue samples obtained via tail biopsy or toe clipping [32]. The tissues were digested by incubation for 1 h at 98 °C in 25 mM NaOH, 0.2 mM EDTA solution. The digested samples were neutralized and centrifuged in 41 mM TRIS–HCl for 5 min in a microcentrifuge at 1500 RCF (~4000 rpm in micro centrifuge with 85 mm rotor). The supernatants, containing the extracted DNA, were collected after centrifugation. The samples can be stored at 4 °C or at −20 °C for longer periods.

PCR primers were ordered from Integrated DNA Technologies Inc., Coralville, Iowa, USA (https://eu.idtdna.com/—last accessed July 2025). The PCR master mix was prepared with the following components: nuclease-free water (Thermo-Fisher Scientific, Waltham, MA, USA, Cat. No. R0581), 10× Taq buffer with KCl (Thermo-Fisher Scientific, Cat. No. B38), 20 μM Forward primer (Mcl1 flox fw. sequence 5′ GGT TCC CTG TCT CCT TAC TTA CTG TAG 3′), 20 μM Reverse primer (Mcl1 flox rev. sequence 5′ CTC CTA ACC ACT GTT CCT GAC ATC C 3′), 25 mM $MgCl_2$ (Thermo-Fisher Scientific, Cat. No. R0971), 2,5 mM dNTP (Thermo-Fisher Scientific, Cat. No. R0181), 5 U·μL^{-1} Taq polymerase (Thermo-Fisher Scientific, Cat. No. EP0402), and the extracted DNA. PCR protocol: 95 °C for 2 min; 35 cycles of: 94 °C for 1 min, 60 °C for 1 min, 72 °C for 1 min; final extension step: 72 °C for 5 min. Samples can be stored at 4 °C. DNA fragments were separated by electrophoresis in a 1.5% agarose gel supplemented with ethidium bromide. A band at 250 base pairs (bp) denotes an Mcl1 +/+ WT mouse, a band at 357 bp denotes an Mcl1ΔMyelo mouse, and bands at both 250 and 357 bp indicate an Mcl1 flox/+ heterozygous mouse (Supporting Information section, Supplementary Materials and Methods, Fig. S1). The PCRs were performed on a Hybaid PCR Express Thermal Cycler (Thermo Electron Corporation/Thermo Fisher Scientific). The gels were documented using Azure C300 Gel Imager (Azure Biosystems, Dublin, CA, USA).

Cardiotoxin-induced sterile inflammation and tissue processing

Sterile muscle inflammation was induced by injecting 50 μL of 12 μM cardiotoxin (CTX) (Latoxan, Portes-lès-Valence, France, Cat. No. L8102-1MG) into both the left and right tibialis anterior (TA) muscles of each examined mouse. Inflamed tissues were isolated and processed at different times after injection, based on the protocol of Guardiola *et al.* [33]. Cell suspensions were prepared by digestion of muscles with collagenase B (Sigma Aldrich, St. Louis, MO, USA, Cat. No. C6885-1G). The suspensions were then purified by filtration through 100 μm and 40 μm cell strainers (PluriSelect, Leipzig, Germany, Cat. No. 43-50 040-51 and 43-50 100-51). The cell suspensions were analyzed by flow cytometry.

Histology

For histological analysis of the spleen, mice were anesthetized with avertin, then transcardially perfused via the left ventricle with a phosphate-buffer solution for 5 min. After this, mice were perfused with 4% paraformaldehyde (PFA) solution in phosphate buffer [34]. The spleens were removed, dehydrated using a series of alcohol solutions, and embedded in paraffin. Sections of 2 μm, 5 μm, 7 μm, and 10 μm thickness were prepared to analyze the spleen's structure. Hematoxylin–eosin and May–Grünwald–Giemsa stains were performed for morphological and cellular studies. 3DHistech PANNORAMIC 1000 scanner was used to scan stained sections, which were then analyzed using 3DHISTECH's QuantCenter 2.3 image analysis platform. Scans were performed with a 40x objective. In the case of May–Grünwald–Giemsa-stained images, the intensity of the red channel in the RGB color space was increased to enhance the visibility of the cytoplasm of the cells.

Flow cytometry analysis

Cell suspensions obtained from different tissues were prepared for flow cytometry analysis. The samples were divided into small aliquots according to the number of stainings. To calculate absolute cell counts, a known number of polystyrene micro particles (8 μm, Sigma Aldrich, Cat. No. 78511) were added to each freshly prepared sample stock before aliquoting. Cells were washed with "FACS buffer" (PBS—pH 7,2—supplemented with 0.5% BSA, 0.05% sodium azide, and 2 mM EDTA) and centrifuged at 500 ***g*** for 3 min. The wash buffer was aspirated and discarded. The cells in residual volume (50 μL) were incubated with TruStain FcX PLUS anti-mouse CD16/32 (BioLegend, San Diego, CA, USA, Cat. No. 156604) and heat-inactivated normal rat serum (Invitrogen, Carlsbad, CA, USA, Cat. No. 10710C) for blocking, followed by the addition of pre-prepared antibody cocktails. Incubation was performed for 30 min on ice in the dark. After the incubation, the cells were washed again. Measurements were performed using ACEA NovoCyte 2000R flow cytometer or BD FACSAria III Cell Sorter or Beckman Coulter CytoFLEX SRT Cell Sorter. Data were analyzed with the FlowJo software (Tree Star/Becton Dickinson, New Jersey, NJ, USA). Monoclonal antibodies for the staining cocktails were pretitrated on normal mouse spleen or bone marrow cells. A detailed list of antibodies and their catalog numbers can be found at the beginning of the Supplementary Materials and Methods, see in Supporting Information section. At least 50 000–100 000 leukocytes ($CD45^+$) were measured per tube for analysis.

SYTO16 green fluorescent cell-permeant nucleic acid stain (S7578, Invitrogen) was applied for staining nucleated erythrocytes and reticulocytes as suggested by the manufacturer (~1:5000 dilution in Ca^{2+}-free physiological saline buffer). Cell nonpermeant "viability" dyes were obtained from Thermo-Fisher Scientific: SytoxAAD (Cat. No. S10349) or 7-AAD (Cat. No. A1310).

Where "positive" and "negative" populations could not be clearly distinguished, fluorescence minus one (FMO) controls were used to fit the gates of interests or draw population boundaries.

The names of the axes and their numerical values on the original flow cytometric plots were rather small; therefore, they were overwritten with larger, more visible text on the result figures. The visible scaling marks were kept to show the same axis scaling for comparison purposes.

Determination and interpretation of the absolute cell count within the examined samples

Absolute cell numbers were determined from flow cytometric measurements with the help of polystyrene microparticles ("counting beads") (8 μm, Sigma Aldrich, Cat. No. 78511), which exhibit characteristically high side scatter (SSC) and uniformly low forward scatter (FSC) (Supporting Information section, Supplementary Materials and Methods, Fig. S2). The number of beads was predetermined by microscopic particle counting using a Bürker chamber. A known number of "counting beads" as added to the sample stocks. The measured cell count was compared with the measured bead count, and the original absolute cell number from the starting sample was calculated based on their ratio. 4.5×10^5 beads were added to the freshly prepared TA muscle cell suspensions from both the left and right sides of the animals. The freshly prepared bone marrow cell suspensions from the left and right femoral bones, as well as the freshly prepared spleen cell suspensions, were supplemented with the same number of counting beads. Blood leukocyte absolute counts were determined from 100 μL blood of the animals in a similar manner, following erythrocyte lysis. The only exception was the determination of mature erythrocyte counts in blood samples, for which 1×10^6 beads were added to 10 μL blood sample to ensure a sufficiently high bead count for accurate erythrocyte calculation.

Blood, bone, spleen, and lymphoid tissue processing for cell characterization

Preparation of cell suspensions from bone marrow, spleen, and blood followed routine protocols previously described by other researchers [35,36]. Briefly, bone marrow cells were obtained from isolated femoral and tibial bones by cutting the epiphyseal region and flushing it through with sterile, ice-cold PBS buffer.

A rapid bone marrow isolation technique was used, involving small (200 μL) capped tubes punctured at the bottom with a fine syringe needle. The epiphyses of the femoral bones were superficially cut at both ends to expose the marrow, and the bones were placed inside the punctured tubes. These tubes—containing the bones—were inserted into larger (1.5 mL) snap-cap tubes and spun in a microcentrifuge. The centrifuge speed was rapidly increased (~10 s) to a maximum of ~13 000 rpm (~16 000 rcf), then allowed to decelerate. The bone marrow pellet was collected from the bottom of the 1.5-mL snap-cap tubes.

Spleen cells were obtained by crushing the tissue with a sterile plastic syringe piston in petri dishes. Cell suspensions were then filtered through 100-μm cell strainers to remove tissue clumps, followed by washing and centrifugation.

Blood samples were collected from the orbital sinus or via cardiac puncture [37]. Cellular components were analyzed by flow cytometry.

Macro photographs of the mouse spleens and bones were taken with a Redmi Note 6 smartphone. Only brightness and contrast were adjusted to enhance existing color differences between samples, using the open source image editor GIMP 2.10 (https://gimp.org/—last accessed July 2025).

Thioglycolate medium-induced peritonitis model

Peritonitis induction followed the protocol described by Lidia et al. [38]. Briefly, peritonitis was induced in mice by intraperitoneal injection of 0.5 mL autoclaved, "aged" (at least 2 months old), 4% thioglycolate medium (Sigma Aldrich, St. Louis, USA, Cat. No. B2551).

On Days 1 and 3 posttreatment, mice were sacrificed and the peritoneum was flushed three times with 8 mL ice-cold phosphate buffer supplemented with 0.5% BSA and 2 mM EDTA. Between flushes, the syringe was attached and detached from the needle without removing the needle from the peritoneum.

The first injected buffer contained a known number of microparticles (4.5×10^5 beads) to facilitate later absolute cell number determination. The collected buffer, containing cells and beads, was centrifuged and prepared for flow cytometry.

Quantitative determination of serum inflammatory cytokine concentrations by sandwich ELISA

Blood samples were collected from WT and Mcl1ΔMyelo mice, and serum was obtained by centrifugation. Samples were stored at −20 °C. The concentration of Serum Amyloid P Component (SAP) was determined using the Mouse Pentraxin 2/SAP Immunoassay kit (R&D Systems, Minneapolis, MN, USA, Cat. No. MPTX20). CXCL1 levels were measured using the Duoset Mouse CXCL1/KC ELISA kit (R&D Systems, Minneapolis, MN, USA, Cat. No. DY453-5). The assay was performed according to the manufacturer's instructions. Samples were diluted 1:200 for SAP measurements and 1:2 for CXCL1 measurements. Optical density was measured at 450 nm using the Synergy HT ELISA Reader, and results were analyzed using Microsoft Excel.

Statistical analysis and data representation

Data analysis was performed using Microsoft Excel and SigmaStat software. Student's t-test was applied for data set comparisons, except when the SigmaStat software recommended an alternative test (e.g., Mann–Whitney U test when the normality test failed).

The GraphPad Prism 6 software was used for data visualization. Error bars in figures represent standard deviations (SD). At least three independent experiments were included in the statistical analyses. Individual data points from independent experiments are represented as circular dots in the bar charts, each corresponding to an examined mouse.

Statistical significance was set at $P < 0.05$. Significance markers were assigned as follows: $*P < 0.05$; $**P < 0.01$; $***P < 0.001$.

Results

Leukocytes in the injured muscle tissue

We examined the leukocyte populations in the processed, injured muscle tissue of Mcl1ΔMyelo mice and their WT counterparts using flow cytometry. In the absence of injury, the healthy tibialis anterior (TA) muscle of the mice contains only a few thousand $CD45^+$ leukocytes. Approximately half of these are $CD11b^+$ (also known as Mac-1) myeloid cells, while the other half are small, non-granulated, CD11b-negative lymphocyte-like cells based on their light scatter properties (data not shown).

We assessed leukocyte numbers in the injured TA muscles at different time points following CTX injection, comparing the differences between WT and Mcl1ΔMyelo mice. The TA muscles were isolated from the injured mice and processed into cell suspensions. The cellular composition of these samples was then evaluated by flow cytometry after staining with various cell-specific, fluorescence-labeled monoclonal antibodies (Fig. 1B,D). As the Gr-1 antibody (clone RB6-8C5) recognizes Ly6G and cross-reacts with Ly6C molecules [39–41], a direct Ly6G specific monoclonal antibody (clone 1A8) was used to detect neutrophil granulocytes. Representative images of the cytometric measurements and gating strategies can be found in the Supplemetary Materials and Methods (Fig. S1), see in Supporting Information section.

The successful induction of tissue injury and inflammation was confirmed by the presence of a large number of neutrophil granulocytes in WT animals. Notable differences in the numbers of immigrating $CD11b^+$ $Ly6G^+$ neutrophil granulocytes were observed one day after muscle injury initiation, persisting on Day 2 postinjury (p.i.) (Fig. 1B,C). The neutrophil count in injured muscle of WT animals sharply decreased by Day 3 (Fig. 1C). The near absence of neutrophils in Mcl1ΔMyelo mice likely contributed to the lower total leukocyte count in their tissue on Day 1 postinjury, as seen in comparisons of $CD45^+$ leukocyte numbers with those of WT mice (Fig. 1A).

We also monitored the appearance of $CD11b^+$ $Ly6G^{negative}$, $Siglec\text{-}F^{negative}$ monocytoid cells in injured muscles (Fig. 1B). These cells were identified as two distinct populations: $Ly6C^{++}$ $F4/80^{low}$ monocytoid cells and $Ly6C^{low}$ $F4/80^+$ macrophage-like cells, as shown in the gating strategy (Fig. 1D). Significant differences were observed in the number of $CD11b^+$ $Ly6C^{++}$ immigrating monocytoid macrophages. The Mcl1ΔMyelo mice had fewer of these cells in inflamed muscle tissue compared to WT counterparts on Days 1 and 2 postinjury (Fig. 1F).

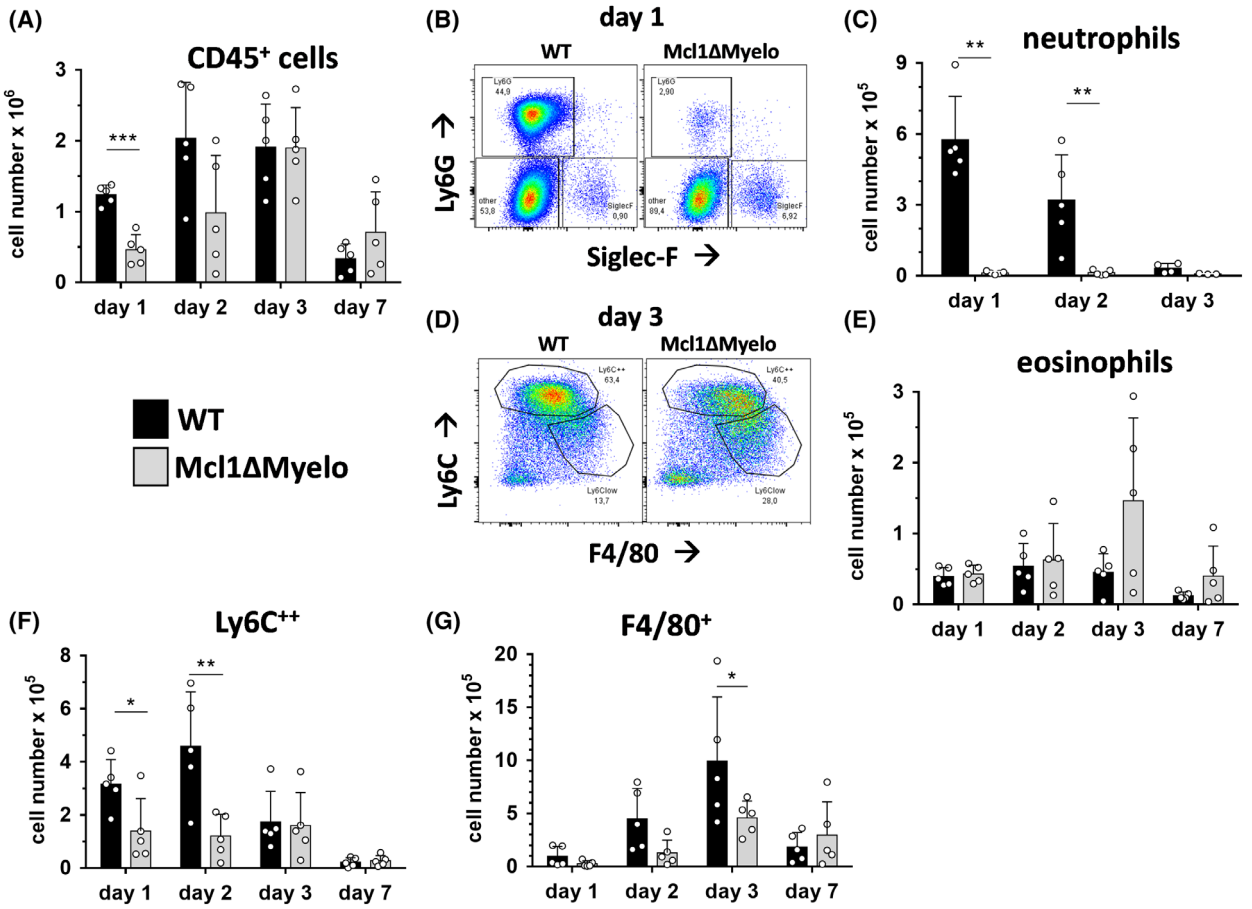

Fig. 1. Comparison of different leukocyte population numbers between WT and Mcl1ΔMyelo mice in injured muscles. (A) Comparison of the number of living $CD45^+$ leukocytes at the indicated time points postinjury. (B) Representative flow cytometric measurements and gating strategy of living $CD45^+$ $CD11b^+$ Siglec-F^+ cells (eosinophils) and living $CD45^+$ $CD11b^+$ $Ly6G^+$ cells (neutrophils) at day 1 post-injury. (C) Comparison of neutrophil granulocyte numbers at Days 1, 2, and 3 postinjury. (D) Flow cytometric measurements of living $CD45^+$ $CD11b^+$ Siglec-F^- $Ly6G^-$ macrophage populations at Day 3 postinjury. (E) Comparison of the eosinophil granulocyte numbers at Days 1, 2, 3, and 7 postinjury. (F) Comparison of the $Ly6C^{++}$ $CD11b^+$ monocytoid macrophage numbers at the indicated time points postinjury. (G) Comparison of $F4/80^+$ $Ly6C^{low}$ $CD11b^+$ macrophage numbers at the indicated time points postinjury. Black bars indicate wild-type (WT) mice, and gray bars indicate Mcl1ΔMyelo mice, as specified. Individual data points, representing sample size per group, are depicted as small circles. Bars display group means, with error bars denoting standard deviation (SD). Statistical significance is indicated as follows: $P < 0.05$ (*), $P < 0.01$ (**), $P < 0.001$ (***).

Additionally, Mcl1ΔMyelo mice exhibited lower numbers of $CD11b^+$ $F4/80^+$ $Ly6C^{low}$ macrophages on Day 3 post-injury compared to WT animals (Fig. 1G). In contrast to other measured myeloid cell types, eosinophil granulocyte numbers were elevated in injured muscles of Mcl1ΔMyelo mice, particularly from Day 3 postinjury. However, the significance of these differences was above the generally accepted probability threshold (Fig. 1B,E).

Elevated T-cell numbers in the injured muscle of Mcl1ΔMyelo animals

On Day 3 postinjury, the $CD45^+$ leukocyte count was similar in the muscles of both the Mcl1ΔMyelo and WT mouse strains (Fig. 1A). However, discrepancies were observed between the measured myeloid cell numbers and the $CD45^+$ leukocyte counts. Unexpected differences in T-cell numbers were found between WT and Mcl1ΔMyelo mice by flow cytometry (Fig. 2).

Compared to WT mice, a significantly elevated number of T cells was counted in the injured muscle samples of neutrophil-deficient Mcl1ΔMyelo mice at all time points examined (Fig. 2). T cells from the injured muscle tissue were identified based on the expression of CD45, CD90, and CD3 molecules with multicolor flow cytometry. CD90 (Thy-1) is expressed by virtually all T cells and is therefore considered a pan-T-cell marker in mice [42]. Using CD90 staining helps to

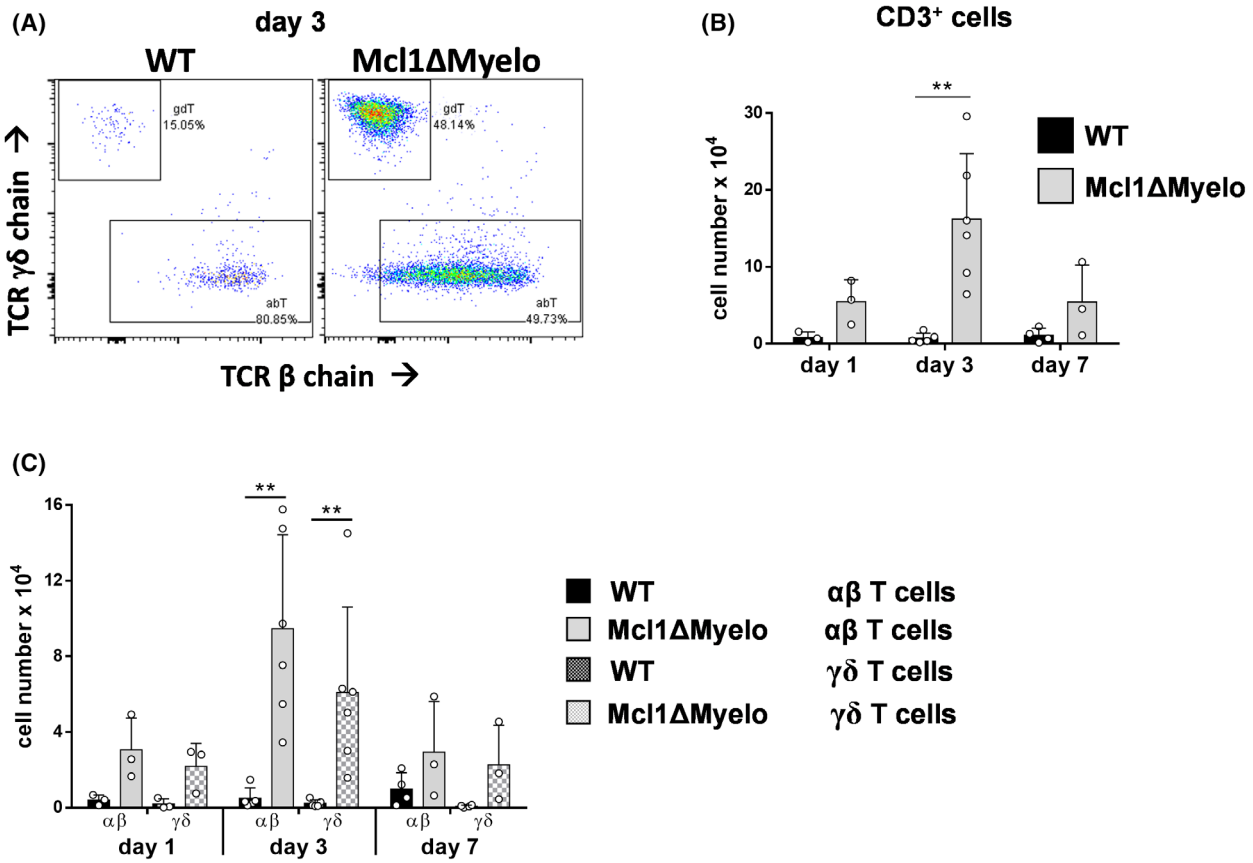

Fig. 2. T cells in injured muscle tissues of WT and Mcl1ΔMyelo mice. Flow cytometry of CD45$^+$ CD90$^+$ CD3$^+$ T cells. (A) Representative flow cytometric measurements of living αβ and γδ T cells at Day 3 postinjury in WT and Mcl1ΔMyelo mice. (B) Living CD3$^+$ T cell numbers in injured tissues of WT and Mcl1ΔMyelo mice at the indicated time points postinjury. (C) Number of αβ and γδ T cell subpopulations at the indicated time points postinjury in the injured tissues. Black bars indicate wild-type (WT) mice, and gray bars indicate Mcl1ΔMyelo mice, as specified. Individual data points, representing sample size per group, are depicted as small circles. Bars display group means, with error bars denoting standard deviation (SD). Statistical significance is indicated as follows: $P < 0.01$ (**).

"shift" the weakly CD3-labeled T-cell population away from nonstained but autofluorescent cells on CD90/CD3 plots, making the identification of T cells clearer and more accurate (See measurement details in Supplementary Materials and Methods, Fig. S4, in Supporting Information section).

The T-cell population can be divided into two separate groups: the TCRβ$^+$ (and TCRγδ$^-$) population representing alpha-beta (αβ) T cells, and the other TCRγδ$^+$ (and TCRβ$^-$) population representing gamma-delta (γδ) T cells (Fig. 2A). We observed an elevated number of both αβ and γδ T cells in the injured muscle samples of neutrophil-deficient Mcl1ΔMyelo mice.

Differences between WT and Mcl1ΔMyelo animals were noticeable as early as Day 1 p.i., reaching borderline significance ($P = 0.055$ for αβ T cells, and $P = 0.053$ for γδ T cells). T cell numbers peaked around Day 3 p.i., with more than a tenfold increase in T-cell count in the injured muscles of Mcl1ΔMyelo mice. These differences were highly significant at this time point (Fig. 2B,C). A difference in T-cell numbers was still observable at Day 7 p.i. The ratio of the γδ T cells was elevated in injured tissue in both WT and Mcl1ΔMyelo mice compared to normal levels in blood circulation, with γδ T cell numbers approaching those of αβ T cells in the injured muscle tissues (Fig. 2C).

Multicolor staining of muscle tissue cells on Day 3 postinjury revealed, on a two-parameter CD3 versus TCRβ plot, that the T cells are clearly heterogeneous (Fig. 3, upper panels). This heterogeneity is especially prominent in Mcl1ΔMyelo mice. Above the TCRβ negative γδ T-cell population, two αβ T cell populations are visible: one with higher TCRβ chain expression but lower CD3 expression (TCRβ^{high}CD3$^+$), and

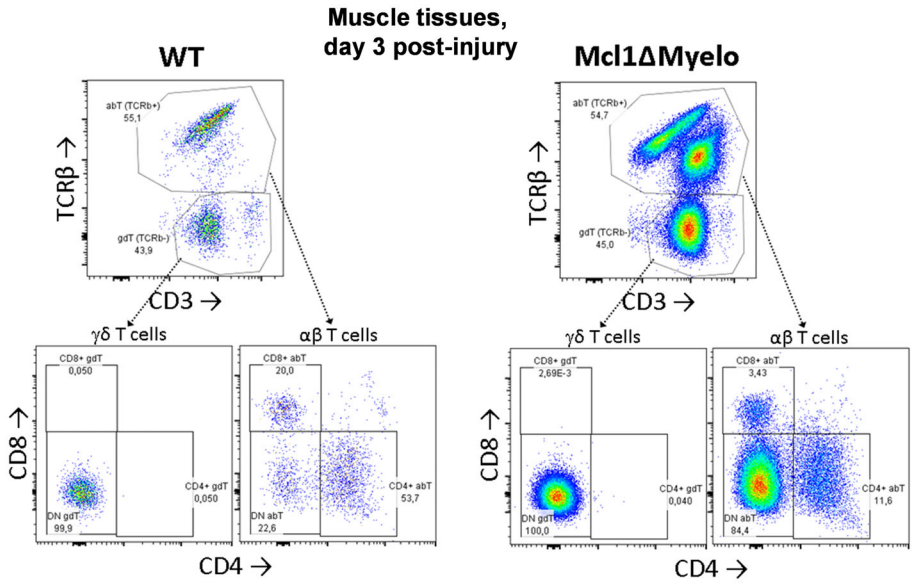

Fig. 3. T cells in injured muscle tissues of WT (left) and Mcl1ΔMyelo mice (right) at Day 3 postinjury. Representative multicolor flow cytometry of CD45$^+$, CD90$^+$, CD3$^+$ T cells. The αβ T cell populations comprise CD4$^+$, CD8$^+$, and double-negative (DN) subpopulations, whereas γδ T cells are double-negative in both WT and Mcl1ΔMyelo mice.

another with slightly lower TCRβ expression but higher CD3 expression (TCRβ$^+$CD3^{high}).

Further analysis of the αβ T-cell composition in injured muscles revealed the presence of both CD4$^+$ and CD8$^+$ T cells. Surprisingly, a considerable number of non-conventional double-negative (CD4$^-$ CD8$^-$, DN) αβ T cells were also present in the injured muscle samples (Fig. 3, lower panels). This DN αβ T cell population is particularly prominent in Mcl1ΔMyelo mice.

Backgating these CD4$^+$, CD8$^+$, and DN subsets of the αβ T cells onto the CD3/TCRβ plot demonstrated that the TCRβ$^+$ CD3^{high} population consists mainly of DN T cells, while the remaining DN T cells co-localize with CD4$^+$ and CD8$^+$ T cells in the TCRβ^{high} CD3$^+$ population. This indicates that the DN αβ T cell compartment itself is heterogeneous (Supplementary Materials and Methods, Fig. S5, in Supporting Information section). Further analysis of the flow cytometry data using alternative gating strategies confirmed the presence of double-negative (DN) αβ T cells within T-cell populations exhibiting varying levels of CD3 expression (Supplementary Materials and Methods, Figs S6, S7, in Supporting Information section).

General differences between WT and Mcl1ΔMyelo mice

We aimed to determine the cause of the remarkable differences in T-cell numbers observed in injured muscles of WT and Mcl1ΔMyelo mice. After considering previously described alterations [2,3], we examined various previously uncharacterized properties of the Mcl1Δmyelo mice.

Since infections or inflammatory conditions can influence various cell types and different components of the immune system, we searched for traces of preexisting inflammation in Mcl1ΔMyelo mice. Using a sandwich ELISA method, we detected an increased concentration of serum amyloid P component (SAP) in the sera of Mcl1ΔMyelo mice (Fig. 4A). SAP belongs to the pentraxin family and is one of the major positive acute-phase proteins in mice [43]. Additionally, the serum CXCL1 concentration was significantly higher in Mcl1ΔMyelo mice compared to WT mice (Fig. 4B). CXCL1 is considered one of the primary neutrophil-attracting IL-8 analogs in mice [44].

We measured several additional inflammation-related cytokines and chemokines, but we did not detect differences in the low serum concentrations of IL-1β, IL-6, and CXCL2 between Mcl1ΔMyelo and WT mice. The examined CCL3 and CCL4 concentrations were below the detection threshold (data not shown).

We also compared the body weight of WT and Mcl1ΔMyelo mice. We measured an equal number of male and female animals within the same age groups (10 and 14 week old animals). Mcl1ΔMyelo mice have slightly, yet significantly lower body weight compared

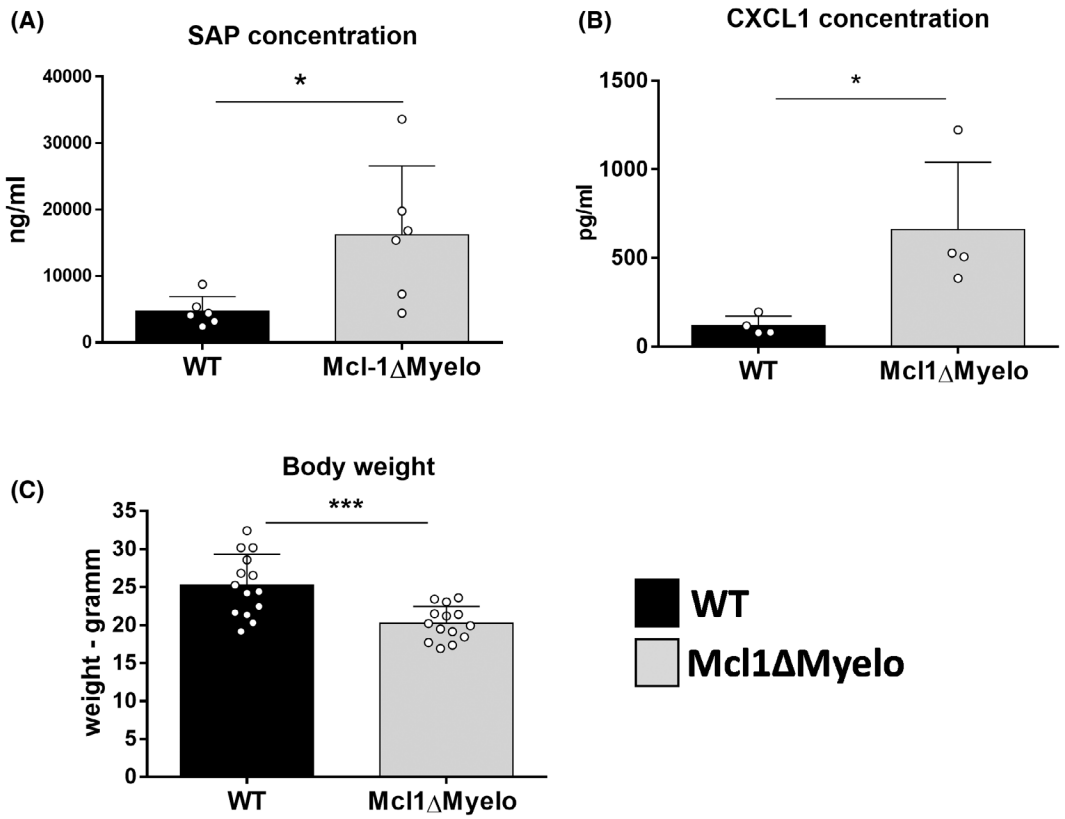

Fig. 4. (A) Serum amyloid P (pentraxin 2) levels in the blood sera of WT and Mcl1ΔMyelo mice. (B) CXCL1 chemokine levels in the blood sera of WT and Mcl1ΔMyelo mice. (C) Comparison of average body weights between WT and Mcl1ΔMyelo mice. Black bars indicate wild-type (WT) mice, and gray bars indicate Mcl1ΔMyelo mice, as specified. Individual data points, representing sample size per group, are depicted as small circles. Bars display group means, with error bars denoting standard deviation (SD). Statistical significance is indicated as follows: $P < 0.05$ (*), $P < 0.001$ (***).

to their WT counterparts (Fig. 4C), which was also mentioned elsewhere [3].

Altered cellular composition in the bone marrow of Mcl1ΔMyelo mice

We observed visible color differences in the femoral and tibial bones between WT and Mcl1ΔMyelo mice (Fig. 5A). The bones of Mcl1ΔMyelo mice appeared paler compared to those of WT animals. This color difference could indicate alterations in either the volume or composition of the bone marrow. Indeed, after isolating the bone marrow from the femoral bones of WT and Mcl1ΔMyelo mice, we observed color differences, but no obvious difference in the volume of the isolated bone marrow samples (Fig. 5B).

We presumed that the discrepancy in T-cell numbers might be linked to altered lymphoid cell development in Mcl1ΔMyelo mice. To clarify this, we investigated the cellular composition of the bone marrow from several WT and Mcl1ΔMyelo mice using flow cytometry (Fig. 6). The number of $CD45^+$ leukocytes was significantly lower in Mcl1ΔMyelo mice than in WT controls ($P = 0.023$) (Fig. 6A).

After cytometric staining, we identified and quantified the number of common lymphoid precursor cells (CLP) and common myeloid precursor cells (CMP) using a well-established protocol that involves several stem cell-associated markers (Supplementary Materials and Methods, Fig. S8, in Supporting Information section) [45–47]. We did not detect significant differences in the number of these precursor cells in the bone marrow of WT and Mcl1ΔMyelo mice (Fig. 6B).

As expected in the Mcl1ΔMyelo mouse model, there was a major difference in neutrophil granulocyte development. The bone marrow of WT animals contained a significantly larger number of conventional $CD11b^+$

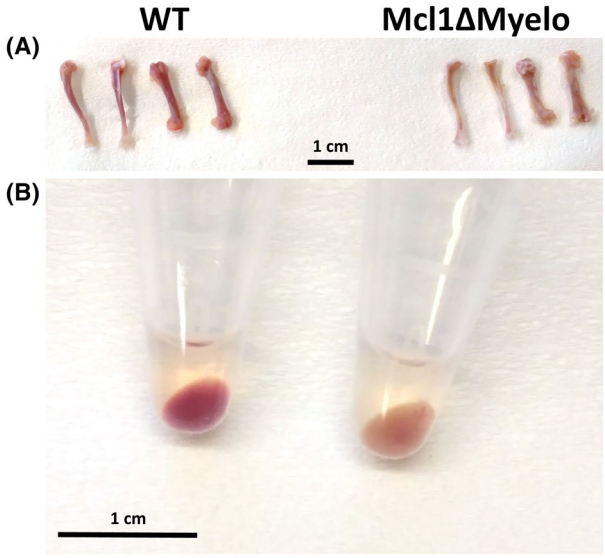

Fig. 5. (A) Representative photograph of tibial bones (left pairs within groups) and femoral bones (right pairs within groups) of WT and Mcl1ΔMyelo mice. (B) Bone marrow obtained from femoral bones of WT and Mcl1ΔMyelo mice after centrifugation in sample tubes. Scale bars in both images represent 1 centimeter (cm).

$Ly6G^{++}$ ($Ly6G^{high}$) $CD125^{+}$ neutrophil granulocytes (Fig. 6C,D). In Mcl1ΔMyelo mice, Mcl1 deficiency obstructs neutrophil granulocyte development [2], leading to the accumulation of a large number of atypical $CD11b^{+}$ $Ly6G^{low}$ $CD125^{+}$ cells in the bone marrow, while only a scarce number of conventional $Ly6G^{++}$ neutrophil granulocytes was observed (Fig. 6C,D). Although this phenomenon was reported in a previous study [2], which used the Ly6G/Ly6C dual-specific Gr-1 monoclonal antibody, it was not emphasized.

We did not detect significant differences in the numbers of $CD11b^{+}$ $Ly6C^{+}$ monocytoid cells, nor were there differences in the numbers of $CD11b^{+}$ Siglec-F^{+} eosinophil granulocytes (Fig. 6E). However, we confirmed a decreased number of $CD19^{+}$ B cells in the bone marrow of Mcl1ΔMyelo mice (Fig. 6F), a finding that was also reported elsewhere [3].

Surprisingly, we observed substantial differences in the numbers of erythroid cell types. The bone marrow of Mcl1ΔMyelo mice contained significantly fewer erythrocytes, reticulocytes, and nucleated erythroblasts compared to WT animals (Fig. 7A,B). These populations were identified based on the presence of Ter119 erythrocyte marker and their nucleic acid content (Supplementary Materials and Methods, Fig. S10, in Supporting Information section). The reduced number of erythroid cells within bone marrow may explain the pale color of the femoral and tibial bones in Mcl1ΔMyelo mice.

Comparison of blood cells

As described elsewhere [2,3], apart from neutrophil granulocytes, there were no differences in the composition of the main cell populations in the blood of WT and Mcl1ΔMyelo mice, including the number of eosinophil granulocytes. We observed an increased number of γδ T cells in the blood of Mcl1ΔMyelo animals. On average, this increase was more than threefold compared to WT controls and was statistically significant (Fig. 8A). Despite the observed differences in the number of erythroid precursors in the bone marrow, we found no significant differences in the numbers of circulating red blood cells, reticulocytes (indicated as pre-RBC), or nucleated erythrocytes (nu-RBC) in the blood of Mcl1ΔMyelo mice compared to WT controls (Fig. 8B).

Altered cellular composition in the spleen of Mcl1ΔMyelo mice

We observed notable differences in spleen size between WT and Mcl1ΔMyelo animals (Fig. 9A). This extreme splenomegaly was frequently observed in aging Mcl1ΔMyelo mice. To quantify these differences, we calculated the spleen-to-body mass ratio for several WT and Mcl1ΔMyelo mice and found significant differences (Fig. 9B).

The increased spleen size and weight suggest alterations in cellular composition. Flow cytometric analysis of spleen cells from WT and Mcl1ΔMyelo mice did not reveal significant differences in the numbers of $CD45^{+}$ leukocytes (Fig. 9C). Similarly, no significant differences were found in the numbers of $CD11b^{+}$ $Ly6C^{++}$ monocytoid cells, $CD11b^{+}$ $F4/80^{+}$ $Ly6C^{low}$ macrophages, or $CD11b^{+}$ Siglec-F^{+} eosinophil granulocytes (Fig. 9D). Additionally, the numbers of αβ and γδ T-cell populations were comparable (Fig. 9E). However, we measured a lower number of $CD19^{+}$ B-lymphocytes in the spleen cell suspension of Mcl1ΔMyelo mice (Fig. 9F), which was consistent with findings in the bone marrow (Fig. 6F).

Surprisingly, we found a large number of atypical $CD11b^{+}$ $Ly6G^{low}$ $CD125^{+}$ neutrophil granulocytes in the spleen of the Mcl1ΔMyelo mice (Fig. 9G), mirroring our observations in the bone marrow (Fig. 6C). This was also observed by others using Ly6G/Ly6C dual-specific Gr-1 antibodies [2]. As expected, the number of $CD11b^{+}$ $Ly6G^{high}$ $CD125^{+}$ conventional neutrophil granulocytes was higher in the spleen of the WT animals than in Mcl1ΔMyelo mice. However, their absolute counts were low in both WT and Mcl1ΔMyelo mice (Fig. 9H).

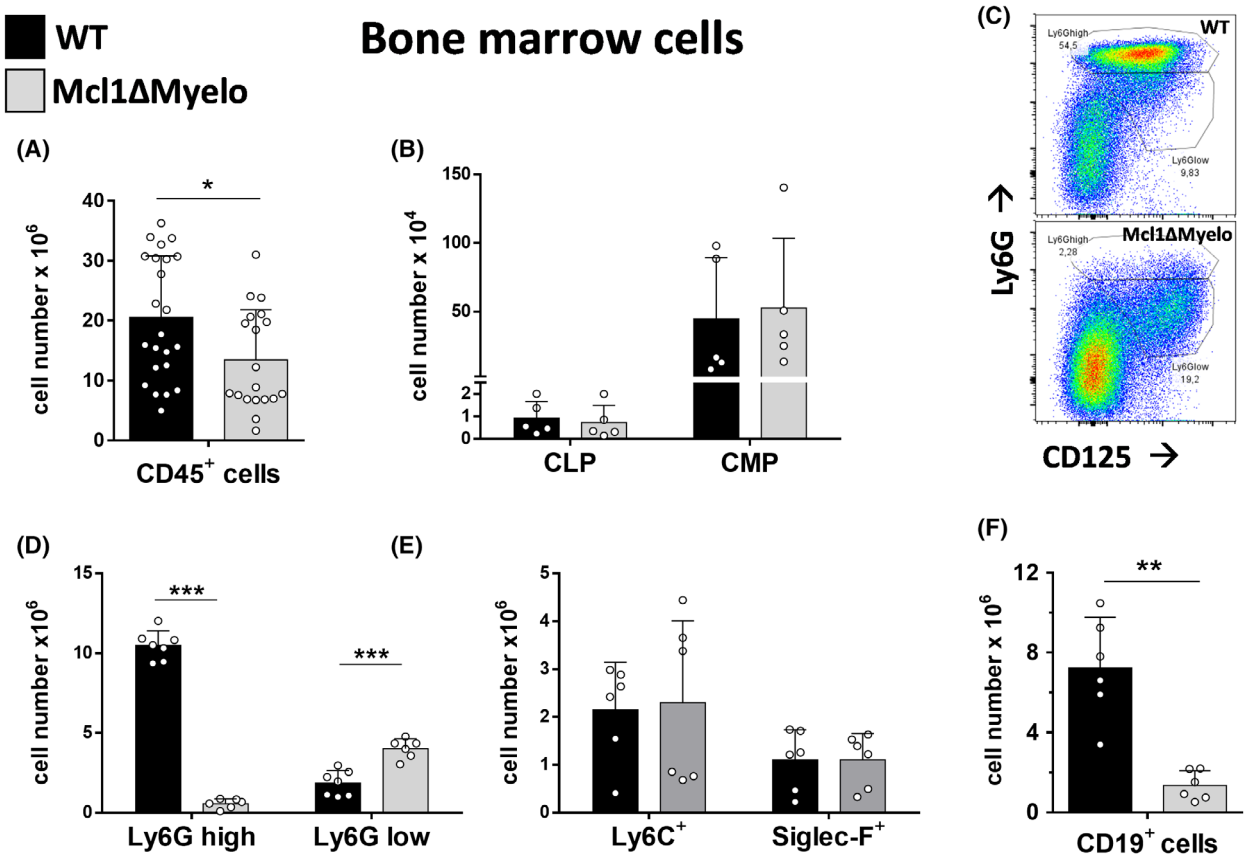

Fig. 6. Comparison of different leukocyte populations between WT and Mcl1ΔMyelo mice in their bone marrow. (A) Comparison of the number of living $CD45^+$ leukocytes. (B) Comparison of common lymphoid precursor (CLP) and common myeloid precursor (CMP) cell numbers. (C) Representative flow cytometric representation of the $CD45^+$ $CD11b^+$ neutrophil granulocytes within the bone marrow of WT and Mcl1ΔMyelo mice. More $Ly6G^{++}$ cells are observed in WT animals. The bone marrow of Mcl1ΔMyelo mice contains a high number of atypical or immature $Ly6G^{low}$ neutrophils. CD125 is the alpha chain of the IL-5 receptor complex. (D) Comparison of classical $Ly6G^{++}$ (Ly6G high) and atypical Ly6G low neutrophil granulocyte numbers. (E) Comparison of $CD11b^+$ $Ly6C^+$ monocytoid cell numbers and $CD11b^+$ $Siglec\text{-}F^+$ eosinophil granulocyte numbers. (F) Comparison of the number of living $CD19^+$ B cells. Black bars indicate wild-type (WT) mice, and gray bars indicate Mcl1ΔMyelo mice, as specified. Individual data points, representing sample size per group, are depicted as small circles. Bars display group means, with error bars denoting standard deviation (SD). Statistical significance is indicated as follows: $P < 0.05$ (*), $P < 0.01$ (**), $P < 0.001$ (***).

The presence of atypical neutrophils suggests that their development may also occur in the spleen of Mcl1ΔMyelo mice. To investigate this, we examined the presence of common lymphoid and common myeloid precursor cells in spleen cell suspensions (see details in Supplementary Materials and Methods, Fig. S9, in Supporting Information section), and found a significantly higher number of CMP cells in the spleens of Mcl1ΔMyelo mice (Fig. 9I). Since CMP cells can give rise to erythroid precursors, we also investigated erythroid cells in the spleen (see details in Supplementary Materials and Methods, Fig. S10, in Supporting Information section). We observed an increased number of nucleated erythroblastoid cells in samples from Mcl1ΔMyelo mice, but without convincing significance ($P = 0.117$) (Fig. 7C,D).

Extramedullary hematopoiesis is commonly observed in rodents in the splenic red pulp [48]. Our findings may indicate extramedullary myelopoiesis in the spleen of Mcl1ΔMyelo mice. To further investigate this, we examined the spleen histology of WT and Mcl1ΔMyelo mice. Spleen tissue sections were prepared from both strains, and 5-μm and 2-μm sections were stained with hematoxylin–eosin or May–Grünwald–Giemsa stains (Fig. 10). Even at low magnification, histological differences were evident between the two strains. The spleen tissue of WT mice exhibited the typical histological architecture, with the red pulp interspersed with nodules of lymphocyte-rich white pulp (Fig. 10A). In contrast, the red pulp of Mcl1ΔMyelo mice appeared structurally different, with a more heterogeneous parenchyma containing

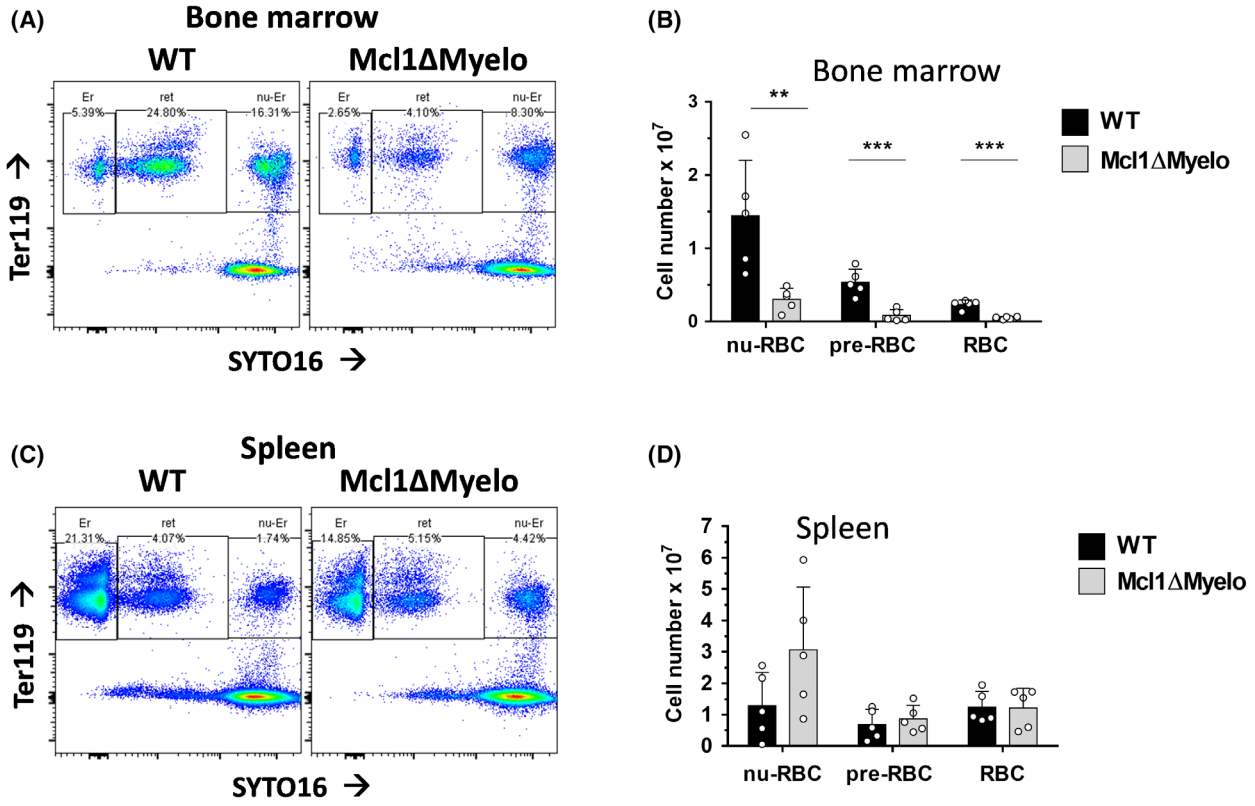

Fig. 7. Erythroid cell types in bone marrow and spleen of WT and Mcl1ΔMyelo mice. Ter119 is considered an erythroid-specific marker. SYTO16 is a cell-permeable fluorescent nucleic acid dye. (A) Representative flow cytometric characterization of the erythroid cell types in the bone marrow of WT and Mcl1ΔMyelo mice. (B) Statistical representation of erythroid cell type numbers in the bone marrow of WT and Mcl1ΔMyelo mice. (C) Representative flow cytometric characterization of erythroid cell types in the spleen of WT and Mcl1ΔMyelo mice. (D) Statistical representation of erythroid cell type numbers in the spleen of WT and Mcl1ΔMyelo mice. Nucleated erythroblasts are indicated as "nu-RBC", reticulocytes as "pre-RBC" and mature red blood cells as "RBC". Black bars indicate wild-type (WT) mice, and gray bars indicate Mcl1ΔMyelo mice, as specified. Individual data points, representing sample size per group, are depicted as small circles. Bars display group means, with error bars denoting standard deviation (SD). Statistical significance is indicated as follows: $P < 0.01$ (**), $P < 0.001$ (***).

fewer, smaller, and irregularly shaped white pulp structures (Fig. 10B).

At higher magnification, the narrow red pulp area of WT mice contained small, uniform cells with dark, heterochromatic nuclei (Fig. 10C). In contrast, the red pulp of Mcl1ΔMyelo mice contained numerous larger, more heterogeneous cell types with thicker cytoplasm and large, lighter euchromatic nuclei (Fig. 10D). Several giant cells were also observed in the spleen of Mcl1ΔMyelo mice.

Increased T-cell numbers in Mcl1ΔMyelo mice in a thioglycolate medium-induced peritonitis model

We aimed to determine whether the elevated T-cell numbers observed in muscle inflammation in Mcl1ΔMyelo mice were specific to muscle injury or reflected a broader inflammatory phenomenon. To investigate this, we induced classical thioglycolate medium-mediated peritonitis in Mcl1ΔMyelo mice and their WT counterparts.

At the examined time points, Day 1 and day 3 post-treatment, T-cell numbers were significantly higher in the inflamed peritoneum of Mcl1ΔMyelo mice compared to WT mice. This increase involved both αβ and γδ T cells (Fig. 11). Notably, Mcl1ΔMyelo mice also exhibited significantly elevated γδ T cell numbers in the peritoneum before thioglycolate treatment (day 0).

Discussion

In this neutrophil granulocyte-deficient mouse model, we observed several differences between WT and

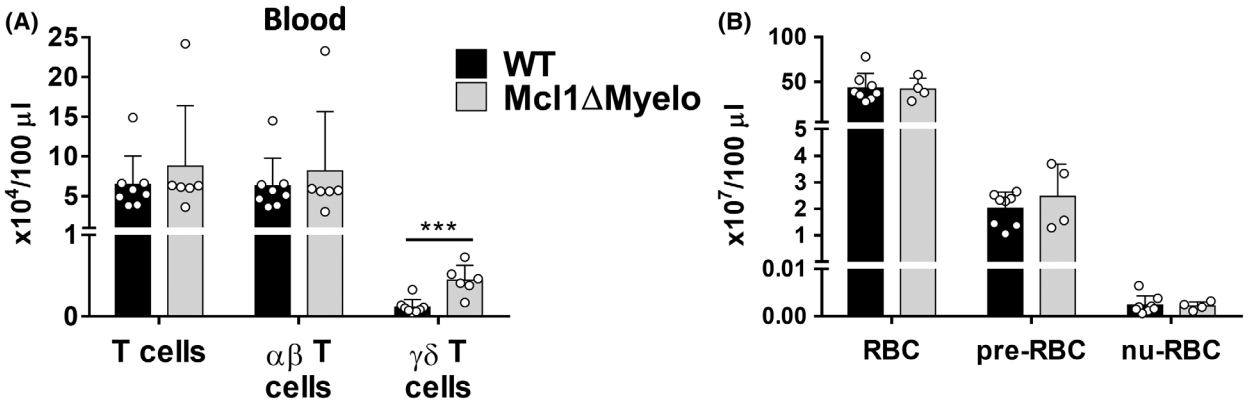

Fig. 8. (A) Cell numbers of the main T cell subpopulations within the blood of WT and Mcl1ΔMyelo mice. (B) There is no significant difference in the number of mature erythrocytes (RBC), reticulocytes (pre-RBC) and nucleated erythroblasts (nu-RBC) in the blood of WT and Mcl1ΔMyelo mice. Black bars indicate wild-type (WT) mice, and gray bars indicate Mcl1ΔMyelo mice, as specified. Individual data points, representing sample size per group, are depicted as small circles. Bars display group means, with error bars denoting standard deviation (SD). Statistical significance is indicated as follows: $P < 0.001$ (***).

Mcl1ΔMyelo mice at both cellular and organ levels. Unexpected differences were seen in the spleen and bones of neutrophil-deficient animals. We observed paler femoral and tibial bones (Fig. 6A), as well as an enlarged spleen in the neutrophil-deficient mice (Fig. 9A). The presence of elevated inflammatory chemokines in circulation (Fig. 4A,B) indicates inflammatory conditions in the body. We speculate that the absence of neutrophil granulocytes makes the gastrointestinal tract or the epidermis vulnerable to subacute infections caused by microbiota. Gastrointestinal inflammatory conditions could negatively influence the gut's nutritional function. These circumstances could potentially explain both the increased SAP and CXCL1 levels (Fig. 4A,B) and the low body weight of the Mcl1ΔMyelo mice (Fig. 4C) [3].

Inflammation mediates increased production of leukocytes, including neutrophils. We suggest that the increased production of neutrophil granulocytes and the accumulation of apoptotic neutrophil precursors in the bone marrow of the Mcl1ΔMyelo mice limit erythrocyte production, indirectly resulting in erythroid cell type-specific bone marrow insufficiency. A low erythrocyte count could induce extramedullary erythropoiesis [49]. During embryonic development, the spleen serves as a hematopoietic organ. In adult mice, remnants of this developmental role can result in baseline extramedullary hematopoietic activity [48], which may be upregulated under specific physiological or pathological conditions [50,51]. This could explain the changes observed in the spleen of the Mcl1ΔMyelo mice. The increased number of CMPs in the spleen (Fig. 9I) gives rise to not only erythrocytes, but also precursors of neutrophils. In the absence of Mcl1, the immature, atypical Ly6G^{low} neutrophils (Fig. 9G,H) likely die inside the spleen, similar to what was observed in the bone marrow (Fig. 7C,D) [2]. The consequence of this increased cell production manifests itself as splenomegaly (Fig. 9A) [52,53]. The atypical structure of the Mcl1ΔMyelo spleen can be easily compared to the regular WT spleen (Fig. 10A,B). At higher magnification, the altered cell composition in the splenic parenchyma is also obvious (Fig. 10C,D).

The absence of infiltrating neutrophil granulocytes in the injured muscle tissue could influence the subsequent inflammatory response and the immune system's regeneration process [54]. A lower number of tissue-immigrating Ly6C^{++} monocytoid cells was observed in the muscle of Mcl1ΔMyelo mice during the first days after tissue injury (Fig. 1F). We hypothesize that the low cell count may be attributed to reduced chemotactic factor production due to the absence of neutrophils.

The appearance of F4/80^{+} Ly6C^{low} macrophages, associated with anti-inflammatory and regenerative functions [31], was delayed and their numbers were also lower in the regenerating muscles of Mcl1ΔMyelo mice (Fig. 1G).

A surprisingly high number of T cells was observed in the injured muscle of Mcl1ΔMyelo mice (Fig. 2). Since the total number of T cells in the blood and spleen did not differ between WT and Mcl1ΔMyelo mice (Figs 8A, 9E), the increased T-cell count in injured muscle may be linked to altered chemotaxis in neutrophil-deficient animals.

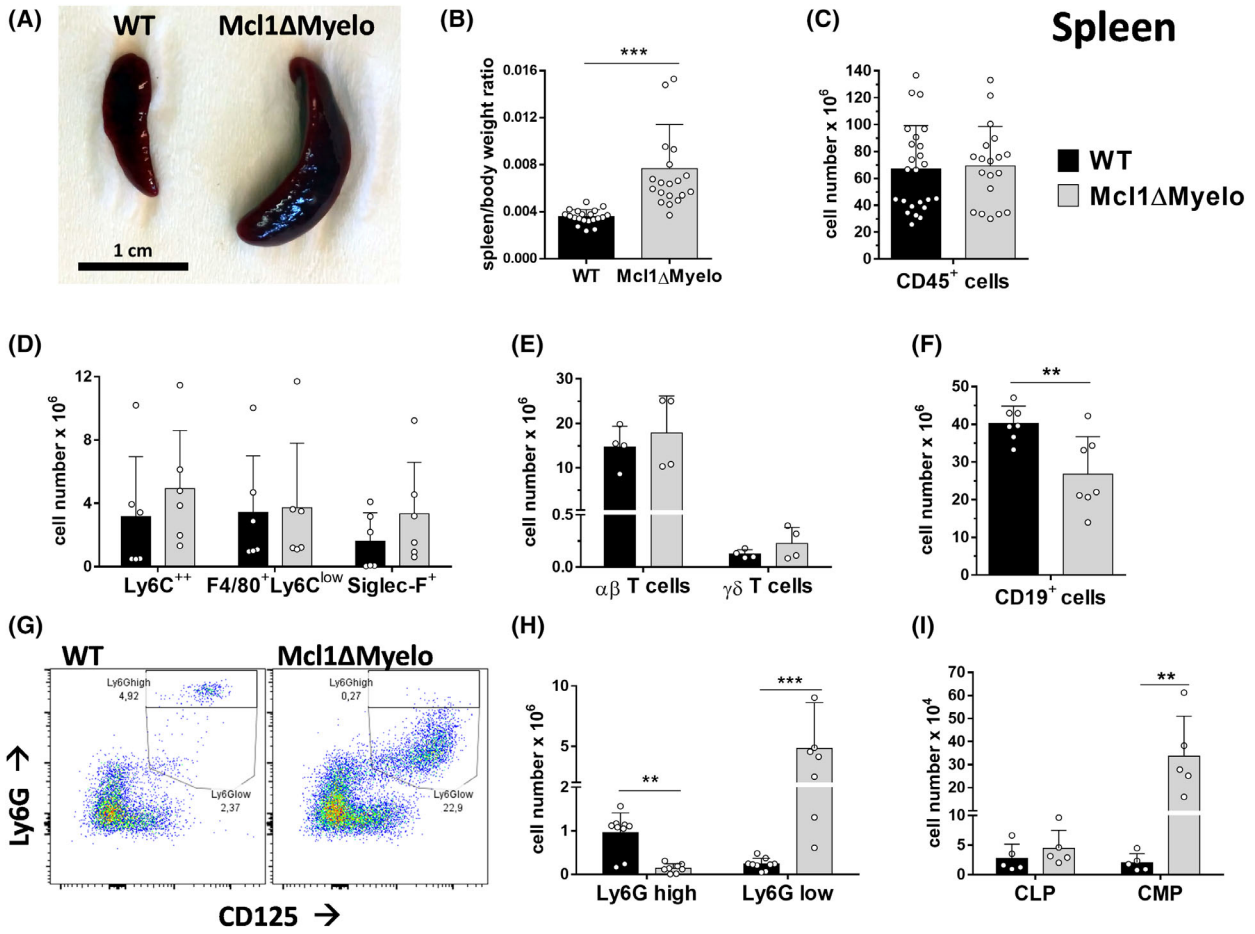

Fig. 9. Comparison of the spleens and the number of different spleen cells between WT and Mcl1ΔMyelo mice. (A) Splenomegaly was observed on several occasions in Mcl1ΔMyelo animals. Scale bar in the photograph represents 1 centimeter (cm). (B) Statistical comparison of spleen/body weight ratio between WT and Mcl1ΔMyelo animals. (C) Comparison of live $CD45^+$ leukocyte numbers. (D) Comparison of $CD11b^+$ $Ly6C^{++}$ monocytoid cell numbers, $CD11b^+$ $F4/80^+$ $Ly6C^{low}$ macrophage numbers, and $CD11b^+$ $Siglec\text{-}F^+$ eosinophil granulocyte numbers. (E) Comparison of αβ T cell and γδ T cell numbers. (F) The number of $CD19^+$ B cells. (G) Representative flow cytometric measurements of live $CD45^+$ $CD11b^+$ Ly6G marker expressing neutrophils in the spleen. Ly6G and CD125 staining help to identify the conventional $Ly6G^{++}$ neutrophils in WT animals, and atypical/immature $Ly6G^{low}$ neutrophils in the spleens of Mcl1ΔMyelo mice. (H) There is a significantly lower number of conventional $Ly6G^{++}$ (Ly6G high) neutrophils in the spleens of Mcl1ΔMyelo mice, but a much higher number of atypical Ly6G low cells. (I) There is a significant difference in the number of common myeloid precursor cells (CMP) in the spleen, but no significant difference in the number of common lymphoid precursor cells (CLP). Black bars indicate wild-type (WT) mice, and gray bars indicate Mcl1ΔMyelo mice, as specified. Individual data points, representing sample size per group, are depicted as small circles. Bars display group means, with error bars denoting standard deviation (SD). Statistical significance is indicated as follows: $P < 0.01$ (**), $P < 0.001$ (***).

We hypothesize that, in WT animals, a substantial number of neutrophil granulocytes extravasate into the injured and inflamed tissue, leading to depletion of chemotactic factors during this process [17–19,55]. In Mcl1ΔMyelo mice, other cell populations expressing similar chemokine receptors or tissue injury sensors are recruited in elevated numbers to the site of tissue injury in the absence of neutrophils.

An alternative explanation could be the absence of arginase enzyme activity in injured muscle of Mcl1ΔMyelo mice due to the lack of neutrophils [27], which may favor the proliferation of extravasating T cells [56].

T cells can influence macrophage activation and function in various ways. For example, activated effector T cells in tissue produce cytokines that modulate or reprogram macrophage differentiation or activity [57]. Stress signals that appear on the surface of macrophages and other tissue cells during injury can activate non-conventional T cells, including γδ T cell

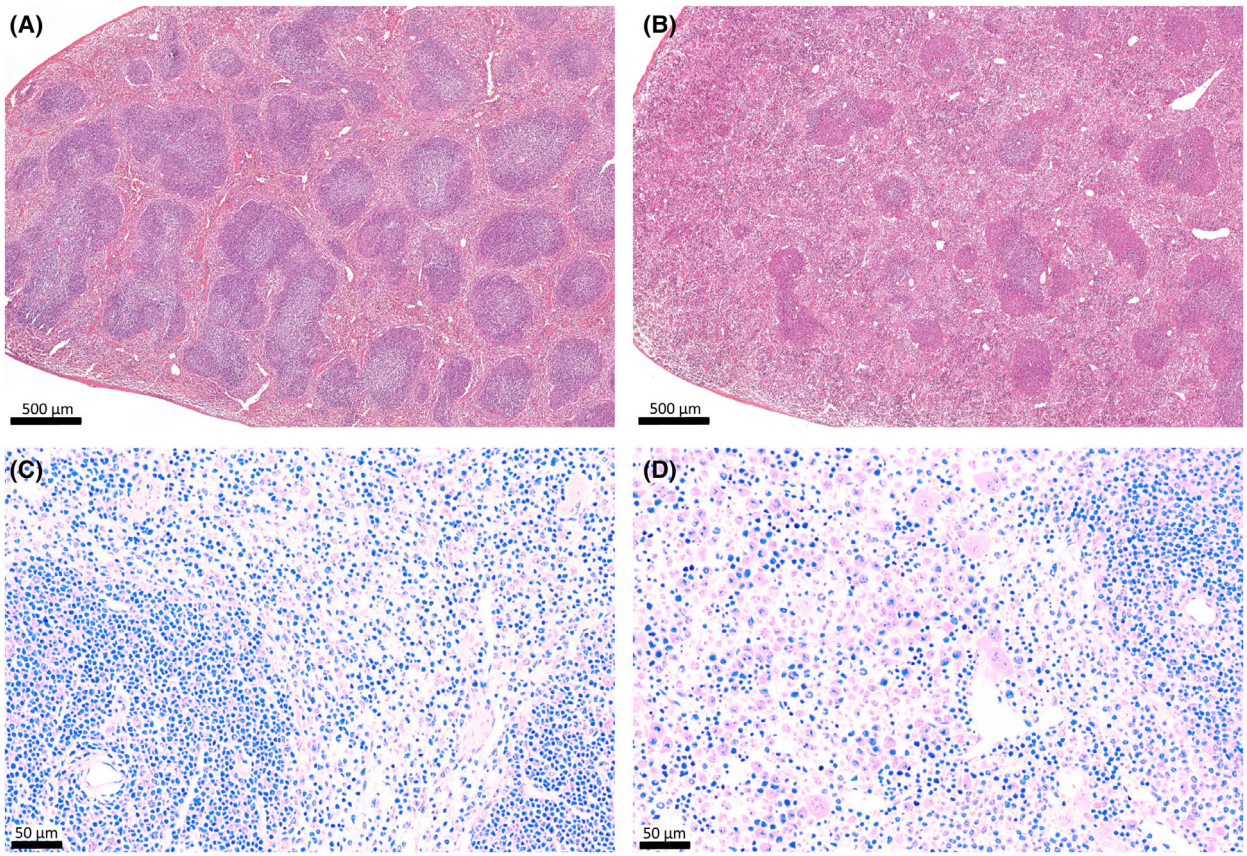

Fig. 10. Microscopic images of spleen tissue sections from wild-type and Mcl1ΔMyelo mice after histological staining. The upper panels (A, B) show low-magnification images of hematoxylin–eosin-stained 5 µm spleen tissue sections from wild-type (A) and Mcl1ΔMyelo (B) mice. The bottom panels (C, D) show higher magnification images of May-Grünwald-Giemsa-stained 2 µm spleen tissue sections from wild-type (C) and Mcl1ΔMyelo (D) mice. The scale bars, indicating lengths of 500 micrometer (µm) in A and B, and 50 µm in C and D, are located at the bottom left corner of each subfigure.

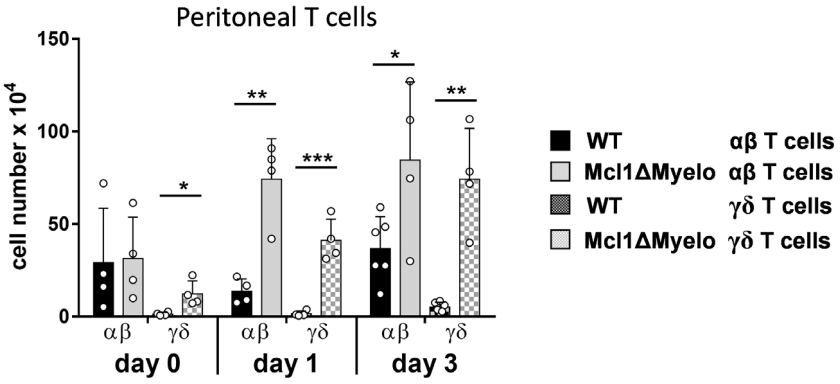

Fig. 11. Comparison of αβ and γδ T cell numbers in the peritonea of WT and Mcl1ΔMyelo mice under baseline conditions (day 0) and at the indicated time points after thioglycolate medium-induced peritonitis. Black bars represent αβ T cells from wild-type (WT) mice; gray bars represent αβ T cells from Mcl1ΔMyelo mice. Black checkered bars represent γδ T cells from WT mice, and gray checkered bars represent γδ T cells from Mcl1ΔMyelo mice, as indicated. Individual data points, representing sample size per group, are depicted as small circles. Bars display group means, with error bars denoting standard deviation (SD). Statistical significance is indicated as follows: $P < 0.01$ (**), $P < 0.001$ (***).

subtypes. The ratio of γδ T cells increases significantly in injured tissues (Fig. 2C) compared to their ratio in the blood and spleen under steady-state conditions. This increase was observed in both wild-type and Mcl1ΔMyelo mice (Fig. 2C). However, in Mcl1ΔMyelo mice, the absolute counts of both αβ and γδ T cells increase substantially (Fig. 2B,C).

It is known that γδ T cells participate in the regeneration of various tissues. For instance, skin γδ T cells produce growth factors (e.g., insulin-like growth factor-1—IGF1) [58,59] during wound healing. It is suggested that IL-17 producing γδ T cells play a role in neutrophil recruitment in CTX induced muscle injury [60]. It has been reported that the number of γδ T cells peaks around Day 3 postinjury in muscles, a finding also confirmed by our data (Fig. 2B). However, neutrophil granulocytes disappear around the same time (Fig. 1C), which challenges the hypothesis that IL-17-producing T cells are responsible for recruiting neutrophil granulocytes to muscle injury. Therefore, we propose that γδ T cells may have alternative immunoregulatory functions and other roles in tissue regeneration.

A high percentage of the αβ T cells in injured muscle consists of nonconventional double-negative (DN) T cells (Fig. 3). Recent studies have described various regulatory and effector roles of DN murine αβ T cells (reviewed in [61,62]); however, their function in CTX-induced muscle injury remains poorly understood. Their elevated count in Mcl1ΔMyelo mice provides an opportunity for further investigation of their properties and their role in tissue inflammation and regeneration.

Elevated T cell numbers were observed not only in muscle injury but also in a conventional inflammation model in Mcl1ΔMyelo mice. The increased T-cell count in thioglycolate medium-induced peritonitis suggests that neutrophil deficiency generally contributes to the enhanced presence of T cells in inflammatory conditions (Fig. 11).

We also observed that the number of eosinophil granulocytes increased similarly to T cells in injured muscles of Mcl1ΔMyelo mice (Fig. 1E). Eosinophils are also recruited by danger signals released during tissue injury [63], and this recruitment may be more pronounced in the absence of neutrophils. The presence of Th2-like effector T cells in severe tissue injuries may produce chemotactic factors that attract eosinophils and vice versa [64]. Cytokines released by eosinophils and T cells (e.g., IL-4) may promote M2-like resolving macrophage differentiation and directly influence muscle precursor cells [65].

The complex immunological and physiological changes manifested in neutrophil-deficient Mcl1ΔMyelo mice during muscle injury and regeneration make it difficult to determine the direct role of neutrophils in these processes. However, we have demonstrated a potential indirect effect of neutrophil deficiency: an increased presence of nonconventional T cells during inflammation and tissue injury. Surprisingly, neutrophil-deficient mice may serve as a useful model for studying the functions and properties of non-conventional T cells in tissue inflammation and repair.

Limitations of the study

We primarily investigated inflammatory events in Mcl1ΔMyelo mice in a descriptive manner, focusing mainly on the cellular level. While acknowledging the importance of macrophages in tissue regeneration, this study focused on the appearance of T cells. Other lymphoid cell types and the functions of macrophage subpopulations were not examined due to resource limitations. The high T cell count observed in Mcl1ΔMyelo mice presents opportunities for future studies, including functional analyses and exploration of T cell transcriptomics and proteomics; however, these analyses are beyond the scope of this study.

We aimed to use an equal number of animals of similar age from both sexes in both WT and Mcl1ΔMyelo experimental groups. However, the inclusion of mixed-sex experimental groups increases the variability of the measured parameters, which primarily increases the probability of a type II statistical error. Therefore, "near-significant" statistical probability values are reported in the text or figures.

Acknowledgements

We gratefully acknowledge the technical assistance of Attila Papp, Dávid Deák, Judit Kállai, Adrienn Gyöngyösi, György Hajas, Zsuzsa Debreceni, Viktória Fedoriska, and Katalin Orosz-Tóth. This study was supported by the National Research, Development, and Innovation Office, Hungary, grant number K 125477.

Author contributions

Conceptualization: HH and PG; Methodology: HH, AP, PG, TV, LSL, AM; Formal analysis: HH, PG; Investigations: HH, PG, TV, AP, LSL; Writing—Original draft preparation: HH, PG; Writing—Review and editing: PG, LN, AM, LSL; Visualization: HH, PG; Supervision: PG; Project administration: PG; Resources: PG, AM, AP, TV; Funding acquisition: TV, LN. All authors reviewed the results and approved the final version of the manuscript.

Peer review

The peer review history for this article is available at https://www.webofscience.com/api/gateway/wos/peer-review/10.1002/1873-3468.70126.

Data accessibility

The data presented in this study are available upon request from the corresponding author.

References

1 McLellan MA, Rosenthal NA and Pinto AR (2017) Cre-loxP-mediated recombination: general principles and experimental considerations. *Curr Protoc Mouse Biol* **7**, 1–12.
2 Dzhagalov I, St John A and He YW (2007) The antiapoptotic protein Mcl-1 is essential for the survival of neutrophils but not macrophages. *Blood* **109**, 1620–1626.
3 Csepregi JZ, Orosz A, Zajta E, Kása O, Németh T, Simon E, Fodor S, Csonka K, Barátki BL, Kövesdi D *et al.* (2018) Myeloid-specific deletion of Mcl-1 yields severely neutropenic mice that survive and breed in homozygous form. *J Immunol* **201**, 3793–3803.
4 Burn GL, Foti A, Marsman G, Patel DF and Zychlinsky A (2021) The neutrophil. *Immunity* **54**, 1377–1391.
5 Mocsai A (2013) Diverse novel functions of neutrophils in immunity, inflammation, and beyond. *J Exp Med* **210**, 1283–1299.
6 Nathan C (2006) Neutrophils and immunity: challenges and opportunities. *Nat Rev Immunol* **6**, 173–182.
7 Soehnlein O, Weber C and Lindbom L (2009) Neutrophil granule proteins tune monocytic cell function. *Trends Immunol* **30**, 538–546.
8 van Gisbergen KP, Sanchez-Hernandez M, Geijtenbeek TB and van Kooyk Y (2005) Neutrophils mediate immune modulation of dendritic cells through glycosylation-dependent interactions between mac-1 and DC-SIGN. *J Exp Med* **201**, 1281–1292.
9 Wittamer V, Bondue B, Guillabert A, Vassart G, Parmentier M and Communi D (2005) Neutrophil-mediated maturation of chemerin: a link between innate and adaptive immunity. *J Immunol* **175**, 487–493.
10 Sheng YR, Hu WT, Chen S and Zhu XY (2024) Efferocytosis by macrophages in physiological and pathological conditions: regulatory pathways and molecular mechanisms. *Front Immunol* **15**, 1275203.
11 Beauvillain C, Delneste Y, Scotet M, Peres A, Gascan H, Guermonprez P, Barnaba V and Jeannin P (2007) Neutrophils efficiently cross-prime naive T cells in vivo. *Blood* **110**, 2965–2973.
12 Puga I, Cols M, Barra CM, He B, Cassis L, Gentile M, Comerma L, Chorny A, Shan M, Xu W *et al.* (2011) B cell-helper neutrophils stimulate the diversification and production of immunoglobulin in the marginal zone of the spleen. *Nat Immunol* **13**, 170–180.
13 Baghdadi MB and Tajbakhsh S (2018) Regulation and phylogeny of skeletal muscle regeneration. *Dev Biol* **433**, 200–209.
14 Tidball JG (2017) Regulation of muscle growth and regeneration by the immune system. *Nat Rev Immunol* **17**, 165–178.
15 Tedesco FS, Dellavalle A, Diaz-Manera J, Messina G and Cossu G (2010) Repairing skeletal muscle: regenerative potential of skeletal muscle stem cells. *J Clin Invest* **120**, 11–19.
16 Hardy D, Besnard A, Latil M, Jouvion G, Briand D, Thépenier C, Pascal Q, Guguin A, Gayraud-Morel B, Cavaillon JM *et al.* (2016) Comparative study of injury models for studying muscle regeneration in mice. *PLoS One* **11**, e0147198.
17 Chen Y, Corriden R, Inoue Y, Yip L, Hashiguchi N, Zinkernagel A, Nizet V, Insel PA and Junger WG (2006) ATP release guides neutrophil chemotaxis via P2Y2 and A3 receptors. *Science* **314**, 1792–1795.
18 de Oliveira S, López-Muñoz A, Candel S, Pelegrín P, Calado Â and Mulero V (2014) ATP modulates acute inflammation in vivo through dual oxidase 1-derived H_2O_2 production and NF-kappaB activation. *J Immunol* **192**, 5710–5719.
19 Huang C and Niethammer P (2018) Tissue damage signaling is a prerequisite for protective neutrophil recruitment to microbial infection in zebrafish. *Immunity* **48**, 1006–1013.
20 Yang D, Han Z and Oppenheim JJ (2017) Alarmins and immunity. *Immunol Rev* **280**, 41–56.
21 Tecchio C, Micheletti A and Cassatella MA (2014) Neutrophil-derived cytokines: facts beyond expression. *Front Immunol* **5**, 508.
22 Yang W and Hu P (2018) Skeletal muscle regeneration is modulated by inflammation. *J Orthop Translat* **13**, 25–32.
23 Lepper C, Partridge TA and Fan CM (2011) An absolute requirement for Pax7-positive satellite cells in acute injury-induced skeletal muscle regeneration. *Development* **138**, 3639–3646.
24 Sambasivan R, Yao R, Kissenpfennig A, Van Wittenberghe L, Paldi A, Gayraud-Morel B, Guenou H, Malissen B, Tajbakhsh S and Galy A (2011) Pax7-expressing satellite cells are indispensable for adult skeletal muscle regeneration. *Development* **138**, 3647–3656.
25 Kovtun A, Scharffetter-Kochanek K, Huber-Lang M and Ignatius A (2018) Neutrophils in tissue trauma of the skin, bone, and lung: two sides of the same coin. *J Immunol Res* **2018**, 8173983.
26 Peiseler M and Kubes P (2019) More friend than foe: the emerging role of neutrophils in tissue repair. *J Clin Invest* **129**, 2629–2639.

27 Bryk JA, Popovic PJ, Zenati MS, Munera V, Pribis JP and Ochoa JB (2010) Nature of myeloid cells expressing arginase 1 in peripheral blood after trauma. *J Trauma* **68**, 843–852.
28 Arnold L, Henry A, Poron F, Baba-Amer Y, van Rooijen N, Plonquet A, Gherardi RK and Chazaud B (2007) Inflammatory monocytes recruited after skeletal muscle injury switch into antiinflammatory macrophages to support myogenesis. *J Exp Med* **204**, 1057–1069.
29 Giannakis N, Sansbury BE, Patsalos A, Hays TT, Riley CO, Han X, Spite M and Nagy L (2019) Dynamic changes to lipid mediators support transitions among macrophage subtypes during muscle regeneration. *Nat Immunol* **20**, 626–636.
30 Kim J and Lee J (2017) Role of transforming growth factor-beta in muscle damage and regeneration: focused on eccentric muscle contraction. *J Exerc Rehabil* **13**, 621–626.
31 Varga T, Mounier R, Patsalos A, Gogolák P, Peloquin M, Horvath A, Pap A, Daniel B, Nagy G, Pintye E *et al.* (2016) Macrophage PPARgamma, a lipid activated transcription factor controls the growth factor GDF3 and skeletal muscle regeneration. *Immunity* **45**, 1038–1051.
32 Jacquot S, Chartoire N, Piguet F, Hérault Y and Pavlovic G (2019) Optimizing PCR for mouse genotyping: recommendations for reliable, rapid, cost effective, robust and adaptable to high-throughput genotyping protocol for any type of mutation. *Curr Protoc Mouse Biol* **9**, e65.
33 Guardiola O, Andolfi G, Tirone M, Iavarone F, Brunelli S and Minchiotti G (2017) Induction of acute skeletal muscle regeneration by cardiotoxin injection. *J Vis Exp* **119**, 54515.
34 Andrews PM and Coffey AK (1984) A technique to reduce fixation artifacts to kidney proximal tubules. *Kidney Int* **25**, 964–968.
35 Kruisbeek AM (2001) Isolation of mouse mononuclear cells. *Curr Protoc Immunol* **39**, 1.
36 Liu X and Quan N (2015) Immune cell isolation from mouse femur bone marrow. *Bio Protoc* **5**, e1631.
37 Parasuraman S, Raveendran R and Kesavan R (2010) Blood sample collection in small laboratory animals. *J Pharmacol Pharmacother* **1**, 87–93.
38 Jimnez-Garca L, Herránz S, Luque A and Hortelano S (2015) Thioglycollate-elicited peritoneal macrophages preparation and arginase activity measurement in IL-4 stimulated macrophages. *Bio-Protocol* **5**, e1585.
39 Fleming TJ, Fleming ML and Malek TR (1993) Selective expression of Ly-6g on myeloid lineage cells in mouse bone-marrow – Rb6-8c5 Mab to granulocyte-differentiation antigen (gr-1) detects members of the Ly-6 family. *J Immunol* **151**, 2399–2408.
40 Sasmono RT, Ehrnsperger A, Cronau SL, Ravasi T, Kandane R, Hickey MJ, Cook AD, Himes SR, Hamilton JA and Hume DA (2007) Mouse neutrophilic granulocytes express mRNA encoding the macrophage colony-stimulating factor receptor (CSF-1R) as well as many other macrophage-specific transcripts and can transdifferentiate into macrophages in vitro in response to CSF-1. *J Leukoc Biol* **82**, 111–123.
41 Daley JM, Thomay AA, Connolly MD, Reichner JS and Albina JE (2008) Use of Ly6G-specific monoclonal antibody to deplete neutrophils in mice. *J Leukoc Biol* **83**, 64–70.
42 Haeryfar SM and Hoskin DW (2004) Thy-1: more than a mouse pan-T cell marker. *J Immunol* **173**, 3581–3588.
43 Bottazzi B, Inforzato A, Messa M, Barbagallo M, Magrini E, Garlanda C and Mantovani A (2016) The pentraxins PTX3 and SAP in innate immunity, regulation of inflammation and tissue remodelling. *J Hepatol* **64**, 1416–1427.
44 Frink M, Hsieh YC, Hsieh CH, Pape HC, Choudhry MA, Schwacha MG and Chaudry IH (2007) Keratinocyte-derived chemokine plays a critical role in the induction of systemic inflammation and tissue damage after trauma-hemorrhage. *Shock* **28**, 576–581.
45 Akashi K, Traver D, Miyamoto T and Weissman IL (2000) A clonogenic common myeloid progenitor that gives rise to all myeloid lineages. *Nature* **404**, 193–197.
46 Challen GA, Boles N, Lin KK and Goodell MA (2009) Mouse hematopoietic stem cell identification and analysis. *Cytometry A* **75**, 14–24.
47 Kondo M, Weissman IL and Akashi K (1997) Identification of clonogenic common lymphoid progenitors in mouse bone marrow. *Cell* **91**, 661–672.
48 Suttie AW (2006) Histopathology of the spleen. *Toxicol Pathol* **34**, 466–503.
49 Cenariu D, Iluta S, Zimta AA, Petrushev B, Qian L, Dirzu N, Tomuleasa C, Bumbea H and Zaharie F (2021) Extramedullary hematopoiesis of the liver and spleen. *J Clin Med* **10**, 5831.
50 Rivera-Torruco G, Muench MO and Valle-Rios R (2024) Exploring extramedullary hematopoiesis: unraveling the hematopoietic microenvironments. *Front Hematol* **3**, 1371823.
51 Ema H, Iseki A, Morita Y and Nakauchi H (2008) Hematopoietic stem cells in the mouse spleen. *Blood* **112**, 2421.
52 Chiu SC, Liu HH, Chen CL, Chen PR, Liu MC, Lin SZ and Chang KT (2015) Extramedullary hematopoiesis (EMH) in laboratory animals: offering an insight into stem cell research. *Cell Transplant* **24**, 349–366.
53 Yamamoto K, Abe-Suzuki S, Abe S, Kirimura S, Onishi I, Kitagawa M and Kurata M (2016) Extramedullary hematopoiesis: elucidating the function

of the hematopoietic stem cell niche (review). *Mol Med Rep* **13**, 587–591.
54 Torres-Ruiz J, Alcalá-Carmona B, Alejandre-Aguilar R and Gómez-Martín D (2023) Inflammatory myopathies and beyond: the dual role of neutrophils in muscle damage and regeneration. *Front Immunol* **14**, 1113214.
55 Calebiro D and Godbole A (2018) Internalization of G-protein-coupled receptors: implication in receptor function, physiology and diseases. *Best Pract Res Clin Endocrinol Metab* **32**, 83–91.
56 Werner A, Koschke M, Leuchtner N, Luckner-Minden C, Habermeier A, Rupp J, Heinrich C, Conradi R, Closs EI and Munder M (2017) Reconstitution of T cell proliferation under arginine limitation: activated human T cells take up citrulline via L-type amino acid transporter 1 and use it to regenerate arginine after induction of Argininosuccinate synthase expression. *Front Immunol* **8**, 864.
57 Orecchioni M, Ghosheh Y, Pramod AB and Ley K (2019) Macrophage polarization: different gene signatures in M1 (LPS+) vs. classically and M2(LPS-) vs. *alternatively activated macrophages*. *Front Immunol* **10**, 1084.
58 Hu W, Shang R, Yang J, Chen C, Liu Z, Liang G, He W and Luo G (2022) Skin gammadelta T cells and their function in wound healing. *Front Immunol* **13**, 875076.
59 Mills RE, Taylor KR, Podshivalova K, McKay DB and Jameson JM (2008) Defects in skin gamma delta T cell function contribute to delayed wound repair in rapamycin-treated mice. *J Immunol* **181**, 3974–3983.
60 Mann AO, Hanna BS, Muñoz-Rojas AR, Sandrock I, Prinz I, Benoist C and Mathis D (2022) IL-17A-producing gammadeltaT cells promote muscle regeneration in a microbiota-dependent manner. *J Exp Med* **219**, e20211504.
61 Wu Z, Zheng Y, Sheng J, Han Y, Yang Y, Pan H and Yao J (2022) CD3(+)CD4(−)CD8(−) (double-negative) T cells in inflammation, *immune disorders and cancer*. *Front Immunol* **13**, 816005.
62 Velikkakam T, Gollob KJ and Dutra WO (2022) Double-negative T cells: setting the stage for disease control or progression. *Immunology* **165**, 371–385.
63 Long H, Liao W, Wang L and Lu Q (2016) A player and coordinator: the versatile roles of eosinophils in the immune system. *Transfus Med Hemother* **43**, 96–108.
64 Spencer LA and Weller PF (2010) Eosinophils and Th2 immunity: contemporary insights. *Immunol Cell Biol* **88**, 250–256.
65 Heredia JE, Mukundan L, Chen FM, Mueller AA, Deo RC, Locksley RM, Rando TA and Chawla A (2013) Type 2 innate signals stimulate fibro/adipogenic progenitors to facilitate muscle regeneration. *Cell* **153**, 376–388.

Supporting information

Additional supporting information may be found online in the Supporting Information section at the end of the article.

Contents of the Supplementary Materials and Methods:

List of antibodies

Fig. S1. Representative example of a genotyping gel.

Fig. S2. (A) The characteristic forward scatter (FSC) and side scatter (SSC) of the counting beads (polystyrene microparticles) are indicated as "beads" on the flow cytometric density plot. (B) The light scattering properties of the measured cells are more clearly visible with a modified SSC axis scale.

Fig. S3. Flow cytometric measurements and representative gating of leukocytes in injured muscle (Day 1 p.i.).

Fig. S4. Determination of T cell subpopulations by flow cytometry.

Fig. S5. Backgating of $CD45^+$ $CD90^+$ $CD3^+$ singlet T cell subsets onto CD3/TCRβ dot plots.

Fig. S6. Gating process of T-cell subsets with different CD3 expression level.

Fig. S7. Backgating of T-cell subsets in injured muscles of Mcl1ΔMyelo mouse (Day 3 p.i.) with different CD3 expression level onto CD4/CD8 plots.

Fig. S8. Measurement of progenitor cells in bone marrow.

Fig. S9. Measurement of progenitor cells in the spleen.

Fig. S10. Determination of erythroid cell types in bone marrow and spleen. Erythroid cells were determined by their light scattering, Ter119 staining and SYTO16 nucleic acid dye staining.